

Toward Real-world Single Image Deraining: A New Benchmark and Beyond

Wei Li*, Qiming Zhang*, *Student Member, IEEE*, Jing Zhang, *Member, IEEE*, Zhen Huang, Xinmei Tian, *Member, IEEE*, and Dacheng Tao, *Fellow, IEEE*

Abstract—Single image deraining (SID) in real scenarios attracts increasing attention in recent years. Due to the difficulty in obtaining real-world rainy/clean image pairs, previous real datasets suffer from low-resolution images, homogeneous rain streaks, limited background variation, and even misalignment of image pairs, resulting in incomprehensive evaluation of SID methods. To address these issues, we establish a new high-quality dataset named RealRain-1k, consisting of 1,120 high-resolution paired clean and rainy images with low- and high-density rain streaks, respectively. Images in RealRain-1k are automatically generated from a large number of real-world rainy video clips through a simple yet effective rain density-controllable filtering method, and have good properties of high image resolution, background diversity, rain streaks variety, and strict spatial alignment. RealRain-1k also provides abundant rain streak layers as a byproduct, enabling us to build a large-scale synthetic dataset named SynRain-13k by pasting the rain streak layers on abundant natural images. Based on them and existing datasets, we benchmark more than 10 representative SID methods on three tracks: (1) fully supervised learning on RealRain-1k, (2) domain generalization to real datasets, and (3) syn-to-real transfer learning. The experimental results (1) show the difference of representative methods in image restoration performance and model complexity, (2) validate the significance of the proposed datasets for model generalization, and (3) provide useful insights on the superiority of learning from diverse domains and shed lights on the future research on real-world SID. The datasets have been released at <https://github.com/hiker-lw/RealRain-1k>.

Index Terms—Single image deraining, real-world derain dataset, domain generalization.

I. INTRODUCTION

IMAGES captured in rainy days suffer from noticeable degradation of visual quality, thereby affecting both human visual perception and practical applications of advanced computer vision systems such as autonomous driving [30], [45]. The aim of single image deraining (SID) is to restore the clean and rain-free background images from the rainy ones. Benefitting from the rapid development of deep convolutional neural networks (CNNs) [19], recent years have witnessed an explosive spread of using CNN models to perform SID [5], [6], [9], [21], [32], [38]–[40].

Recently, many research efforts have been made to solve SID from synthetic images to the real-world rainy images, where two real datasets are proposed, *i.e.*, SPA-data [32] and RainDS [27]. While they contribute to advancing the research for real-world SID, the difficulty in collecting high-quality rainy and clean pairs in the real world leads to various issues, including low resolution (256×256), homogeneous

rain streaks, limited background variation (Figure 1 (b)), and even spatial misalignment (Figure 1 (a)), limiting the generalization ability of SID models trained on them in dealing with various real-world rainy images and implying limited practical significance of them.

As a result, there are several important research questions that have not been well studied or even remain unexplored: 1) How the existing SID methods perform in complex real-world scenarios, where the rainy images are captured at high resolutions and have diverse rain streaks and backgrounds? 2) How about the quantitative performance of existing methods when generalizing to an unseen real scene? 3) How to well utilize existing large-scale synthetic datasets to obtain a better performance on real rainy images?

To answer these questions, it is necessary to establish a new high-quality real-world dataset and pave the way for future research in this field. In this paper, we make an attempt towards this goal by proposing two datasets, RealRain-1k and SynRain-13k. Specifically, we first collect 1,120 high-resolution rainy videos, covering different scenes with diverse rain streaks and abundant backgrounds. Then, we use a simple yet effective method to control the rain density in our generated images and carefully check their spatial alignment. In this way, we obtain 1,120 high-quality image triplets (of clean, light rain, heavy rain), resulting in two versions of our RealRain-1k dataset, *i.e.*, RealRain-1k-L and RealRain-1k-H, respectively.

Besides, RealRain-1k also provides abundant real rain streak layers as a byproduct by reversing the linear superimposition model on clean and rainy images. We thus construct a large-scale synthetic dataset named SynRain-13k by pasting the rain streak layers on abundant natural images. It has a smaller domain gap to real rainy images compared with previous synthetic datasets, thereby facilitating training better SID models.

Based on RealRain-1k and SynRain-13k, we benchmark more than ten SID models on three tracks: 1) SL track, where these models are trained and evaluated on RealRain-1k in a supervised learning manner. We compare their performance in terms of restoration quality, model complexity, inference throughput, and convergence speed; 2) DG track, where these models are trained on different datasets and tested on unseen real datasets to investigate their syn-to-real and real-to-real domain generalization ability as well as the value of synthetic datasets; 3) TL track, where SID models are pre-trained on synthetic datasets, further fine-tuned and tested on real datasets to investigate the benefit of transfer learning. Based on the experiment results, we gain some useful insights on the limitations of existing SID methods and datasets and discuss

*Equal contribution.

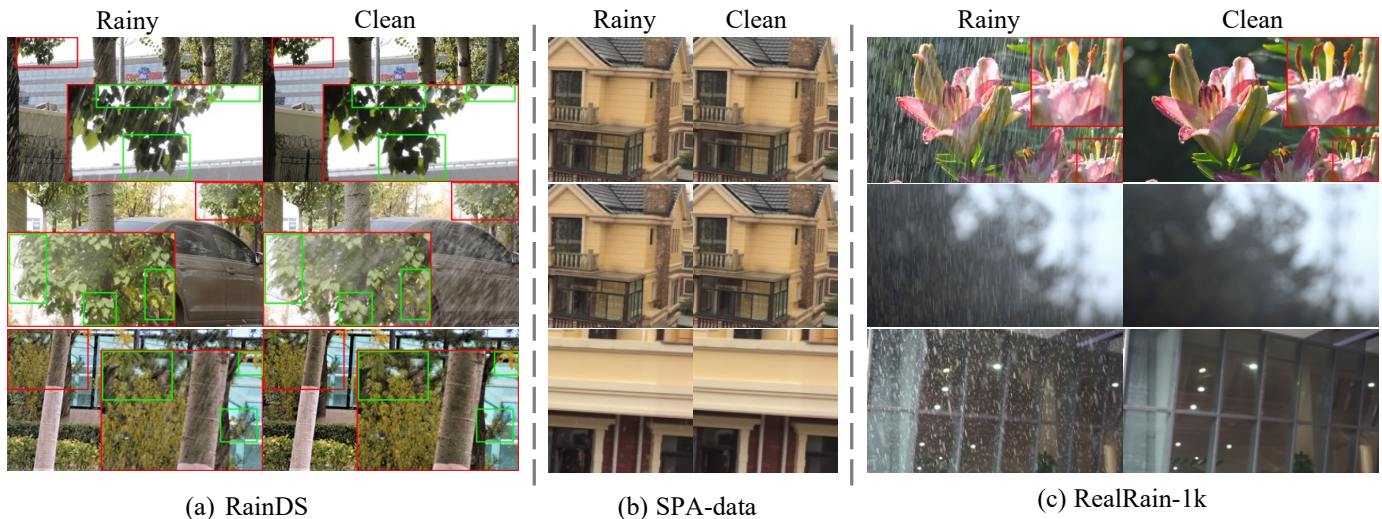


Fig. 1. A glance at different real rainy datasets. (a) RainDS. (b) SPA-data. (c) our RealRain-1k. The image patches in red rectangles are enlarged for better visual comparison. Some misaligned regions in RainDS are indicated by green rectangles. The diversity of rain streaks and background appearance in SPA-data is relatively limited.

future research directions.

The main contribution of the paper is two-fold. (1) We establish a high-quality real dataset RealRain-1k for SID study, which consists of 1,120 high-resolution clean and rainy image pairs with diverse rain streaks, abundant backgrounds, and strict spatial alignment. We also generate a large-scale synthetic dataset of 13k image pairs, *i.e.*, SynRain-13k, by leveraging the diverse real rain layers from RealRain-1k. (2) Based on them, we comprehensively benchmark more than ten representative SID methods on three tracks including SL, DG and TL. The experiment results validate the value of our datasets and provide useful insights on the limitations of existing SID methods.

II. RELATED WORK

A. Single image deraining

Traditional methods Generally, SID methods can be categorized as prior-based methods and data-driven deep learning ones. Traditional methods mainly use hand-crafted features and priors to describe the features of rain streaks. For example, Kang et al. [17] propose to first decompose an image into low and high frequency parts and remove rain streaks in the high frequency layer via dictionary learning. Luo et al. [26] present a discriminative sparse coding method for separating rain streaks from the background. Li et al. [22] use Gaussian mixture models (GMM) as the prior to model rain streaks and background separately for rain removal. Zhu et al. [47] utilize layer-specific priors to discriminate rainy regions. Albeit achieving good performance on certain scenarios, the prior-based methods rely on specific priors, which may not applicable to many real scenes where the rain streaks are complex and diverse. As a result, they have a limited generalization ability.

CNN-based methods Recently, many deep-learning based approaches [1], [2], [6], [9], [15], [16], [21], [28], [31], [32],

[36]–[38], [46], have been proposed for rain streak removal and made significant progress in this area. For example, Fu et al. first adopt a shallow CNN [8] and then a deeper ResNet [9] to remove rain streaks. Zhang et al. [42] take the rain density into account and present a multi-task CNN for joint rain density estimation and deraining. Ren et al. [28] provided a simpler baseline deraining network by considering network architecture, input and output, and loss functions. Jiang et al. [16] proposed a multi-scale coarse-to-fine progressive fusion network to remove rain streaks.

Transformer-based methods Vision transformer [7], [29] has recently been introduced in image restoration tasks and obtains significant performance due to its powerful modeling ability [3], [14], [18], [24], [35]. Chen et al. [4] first applies a standard transformer block equipped with multiple heads and tails for multiple low-level vision tasks including deraining. Liang et al. [23] propose a Swin Transformer-based model by combining CNN and transformer and achieves superior performance while maintaining computational efficiency. Wang et al. [34] constructs a U-shape transformer based on Swin Transformer for image restoration. Apart from the U-shape architecture, Restormer [39] utilizes the channel-wise attention and convolution and obtains better SID results.

B. Deraining datasets

Multiple datasets for SID have been proposed in previous works [9], [13], [20], [22], [36], [43], [44], most of which are generated by first creating rain streaks using the photo-realistic rendering technique [11], [12] and then blending them with clean images. For example, Jiang et al. [16] propose a large and diverse synthetic dataset containing 13k paired images gathered from multiple aforementioned datasets. As for real data, there are two paired datasets in this field as far as we know, named SPA-data [32] and RainDS [27], respectively. When revisiting the rainy images in RainDS, we

find that they are generated by using sprinklers in front of the camera to simulate the rainy scenes, leading to depth information loss and homogeneous rain streaks due to the less-varied rain-to-camera distance and the less-varied physical characteristics of the water from sprinklers. We also identify the spatial misalignment issue in RainDS as indicated by the green rectangles in Figure 1 (a), which will cause erroneous loss that misleads the training process and result in inaccurate evaluation performance. The rainy images in SPA-data are the frames from 170 videos with static backgrounds, among which drizzling videos are dominating. Consequently, the small number of videos and sparse rain streaks in each image lead to the limited diversity of rain and background appearances as shown in Figure 1 (b), which cannot comprehensively reflect the complex and diverse scenes in real world with rain at various densities. Besides, the images in SPA-data are small patches with low resolution as shown in Table I. Although these two datasets have advanced the research in this field, there are still some problems needed to be solved. On the one hand, due to the domain gap between synthetic and real rainy images, SID models trained on existing synthetic datasets always do not generalize well on real-world rainy images. On the other hand, existing real-world datasets have limited diversity in rain streaks, backgrounds, and scenes, making it difficult to benchmark SID methods comprehensively. Therefore, it is necessary to establish a high-quality real-world dataset containing abundant scenes, diverse rain streaks, and various rain densities, and benchmark existing methods to show the overall progress in this area.

III. THE PROPOSED DATASETS

A. The real rainy dataset: RealRain-1k

Data collection We first collect a large number of high-resolution rainy videos from diverse real-world scenes. Specifically, 972 high-resolution rainy videos with static background are captured using a tripod to avoid the jittering artifacts and achieve strict spatial alignment. Moreover, we also collect 148 online available videos and have 1,120 videos in total, which cover various daylight and night outdoor scenes such as buildings, avenues, and parks. In addition, they have diverse rain streaks, different rain densities, and various backgrounds.

Triplet generation We notice that the rain in the real world significantly varies from light to heavy. To this end, we use a simple yet effective rain density-controllable filtering method to generate rainy and clean image pairs with different rain densities to mimic different rainy scenarios in the real world. The process is illustrated in Figure 2. Based on the observation that the pixel in a rainy image always has higher intensity if covered by rain streaks, we propose a simple maximum filtering method over the video clips to select and retain the bright pixels, *i.e.*, pixels with rain. Specifically, given the pixel intensity $P_{(x,y)}^i$ at the position (x, y) of the i_{th} frame from a rainy video, the rainy images R are generated as follows:

$$R_{(x,y)} = \max\{P_{(x,y)}^i | l \leq i \leq r\}, \quad (1)$$

where l and r denote the selected start and end frame index in the video. Obviously, if a longer video clip is selected in

Eq. (1) (*i.e.*, a larger $|r - l|$) for rainy image generation, more pixels covered by rain streaks will be kept and thus the rain density increases, and *vice versa*. In this way, we can mimic the real-world rainy images with various rain densities by simply adjusting the length of the selected video clip to control the rain density in the generated rainy images. Specifically, we generate rainy images with two levels of rain densities, *i.e.*, light and heavy, respectively, where the clip length is determined manually for each video since our captured videos have different rain densities. Figure 4 shows some examples with different rain densities.

It is assumed that the pixel is infrequently covered by rain streaks in a video clip lasting for a long period, especially in the mild rainy conditions. Thereby, most pixels at the same spatial position of the consecutive frames may be clean pixel candidates. Based on this assumption, we propose a simple median filtering method to obtain a reference clean (background) image for each video. Specifically, let $B_{(x,y)}$ denotes the pixel value at the position (x, y) in the generated clean image, it can be calculated as follows:

$$B_{(x,y)} = \text{median}\{P_{(x,y)}^i | l \leq i \leq r\}, \quad (2)$$

where $P_{(x,y)}^i$, l , and r have the same meanings as Eq. (1).

To obtain high-quality rainy and clean image pairs, we carefully check them during the generation process. Three rounds of cross-checking and re-generation (*e.g.*, select the start frame index and adjust the length of the video clip) are carried out to ensure the quality of the generated image pairs, *i.e.*, in terms of strict spatial alignment, clean images without rain streaks, various rain streak appearances, and diverse backgrounds. In total, we generate 1,120 image triplets (clean, light rain, heavy rain) respectively for two versions of our RealRain-1k dataset, *i.e.*, RealRain-1k-L and RealRain-1k-H respectively.

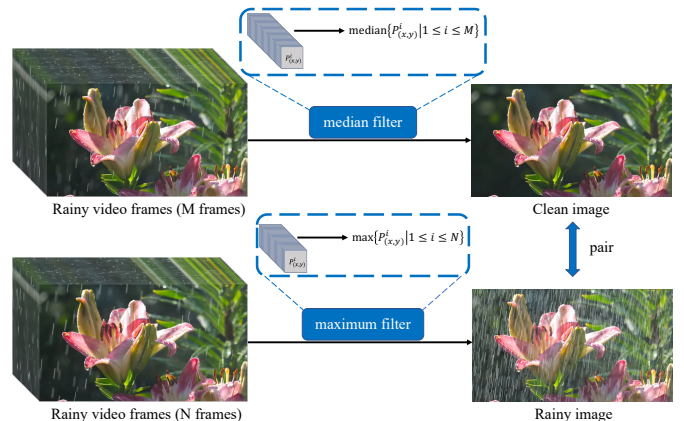


Fig. 2. Overview of the generation pipeline of RealRain-1k.

How to avoid the misalignment issue? It's difficult to capture high-quality rainy and clean pairs with exact the same scene at the same time. We thus conduct the following strategies to guarantee the alignment quality in RealRain-1k: 1) Many images in our dataset consist of static objects (such as buildings, cars, etc.) that will not be affected when rain-drops hit. 2) Thanks to the proposed rain density-controllable

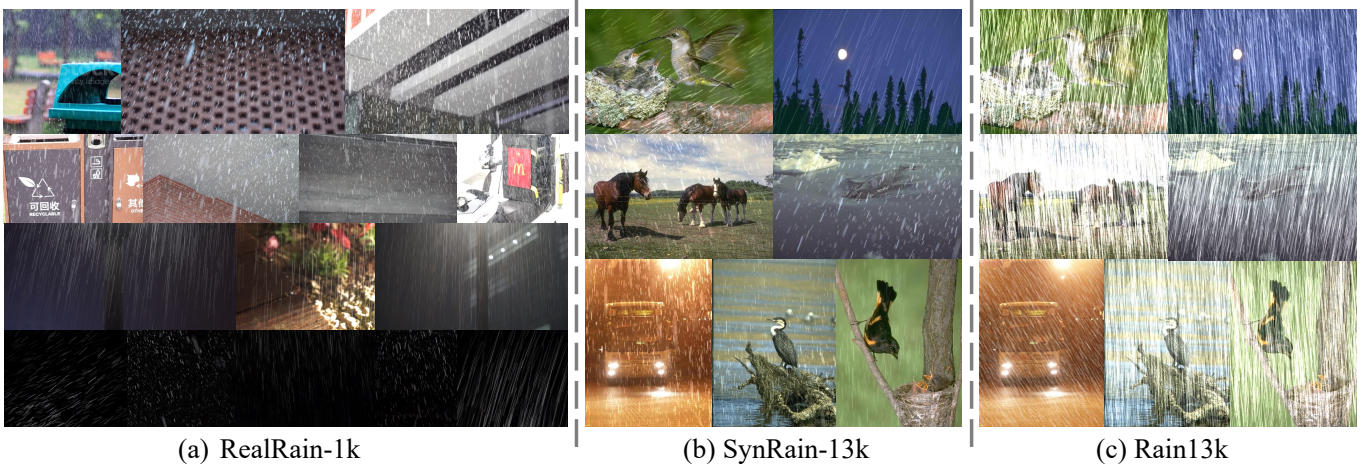


Fig. 3. Some examples from our RealRain-1k, SynRain-13k, and Rain13k [16]. We show some real rain layers from our RealRain-1k in the bottom row of (a). We choose the rainy images with the same backgrounds from our SynRain-13k and Rain13k for a better comparison.

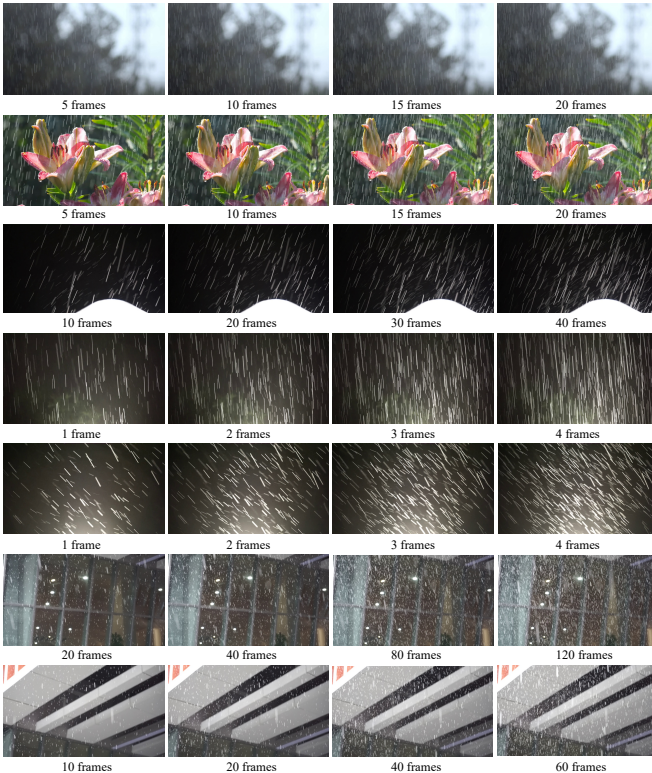


Fig. 4. Some rainy images with different rain densities generated by the proposed method. The number below each image denotes the number of frames used for generating the rainy image based on the maximum filter.

generation method, we don't have strict weather limitations to obtain the rainy videos with diverse rain densities. We instead choose the relatively normal rainy days to reduce the impact of the raindrops hitting the easy-to-move objects (flowers, leaves, etc.). Similarly, breezy days are selected to avoid wind disturbance. 3) We also carefully filter out some video clips with large disturbances (caused by wind, rain, and human disturbances) with many human efforts to ensure the quality of the dataset regarding alignment. Then each pair in our

dataset undergoes repeated (at least three times) comparisons between rainy images and groundtruth. If disturbances are still unavoidable after filtering out the undesirable video clips, we choose to throw away the pairs from our dataset.

We acknowledge that it is impossible to obtain completely aligned real rainy datasets, and thus we made many efforts to include strict human supervision in the loop to make the misalignment almost invisible to the naked eyes. Compared to current valuable real rainy datasets SPA-data and RainDS, the misalignment issue is relieved in RealRain-1k. It is noted that we don't claim the alignment issue is completely resolved and don't mean to criticize existing real datasets. They have played an important role in promoting the development of real-world SID. We just hope RealRain-1k can make a positive supplement to the existing real rain datasets and our work can help to shed some light on the community of real-world SID. **Data organization and statistics** The 1,120 image pairs in RealRain-1k-L (and RealRain-1k-H) are further split into three disjoint subsets, *i.e.*, training set, validation set, and test set, at the ratio of 7:1:2 respectively. Compared with SPA-data and RainDS, our RealRain-1k contains higher resolution images, *i.e.*, an average resolution of $1,512 \times 973$. Some examples are shown in Figure 3 (a) and Figure 6. The statistics of the proposed RealRain-1k and previous representative datasets are summarized in Table I.

B. The synthetic rainy dataset: SynRain-13k

As a byproduct, we can extract the real rain layers from the rainy images in the training set of RealRain-1k-L after obtaining the rainy and clean image pairs. As shown in Figure 5, it can be achieved by reversing the linear superimposition model as follows:

$$L = R - B, \quad (3)$$

where R and B represent the rainy and clean images, respectively. After double-checking the appearances and density of the extracted rain streaks, we manually select 440 clean rain streak layers finally. Some examples are shown in the bottom row of Figure 3 (a). Then, we randomly paste them

TABLE I

THE COMPARISON OF THE PROPOSED REALRAIN-1K AND SYNRAIN-13K DATASETS AND EXISTING ONES. THE NUMBER SEPARATED BY THE SLASHES IN THE SECOND COLUMN DENOTES THE NUMBER OF IMAGE PAIRS IN THE TRAINING SET, VALIDATION SET, AND TEST SET IN EACH DATASET, RESPECTIVELY.

Dataset	Image pairs	Data source	Real	Average resolution	Features	Ratio of night scenes
RainDS [27]	150/0/98	using sprinkler	✓	1,296×728	not strictly aligned, homogenous rain streaks	0%
SPA-data [32]	638,492/0/1,000	170 videos 49% videos are captured using mobile phone	✓	256×256	mostly light rain, homogeneous rain streaks	7.53%
Rain13k [16]	13,711/0/4,298	synthetic rain streaks and background images	✗	482×420	large domain gap between real and synthetic	-
RealRain-1k	784/112/224	1,120 high-resolution videos 87% videos are captured using SONY digital camera	✓	1,512×973	strictly aligned, diverse rain streaks, controllable rain density	47.95%
SynRain-13k	13,711/198/1,200	real rain layer + background	✗	482×420	small domain gap between real and synthetic	-

on the clean images from Rain13k [16] following the linear superimposition model and the process is illustrated in Figure 5. In this way, we generate a new large-scale synthetic rainy dataset containing 13k rainy images, *i.e.*, SynRain-13k, by keeping the same dataset volume as Rain13k. Compared with previous synthetic datasets that are generated based on simulated rain streaks [25], [36], we directly use the real rain layers, thereby reducing the domain gap between the synthetic and real images, which is never explored before. Some examples are shown in Figure 3 (b). As demonstrated in the experiment parts, SID models trained on our SynRain-13k show better generalization performance on real rainy images.

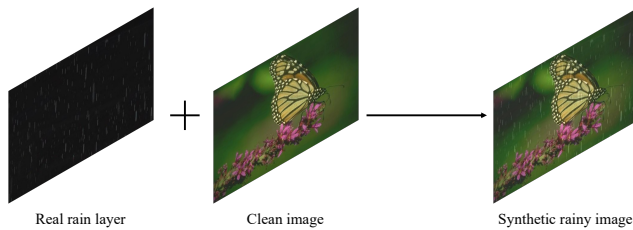


Fig. 5. Overview of the generation pipeline of SynRain-13k.

IV. EXPERIMENTS

Based on our proposed real and synthetic datasets RealRain-1k and SynRain-13k, we benchmark thirteen representative SID methods including two traditional ones [22], [26] and eleven state-of-the-art deep learning-based ones [5], [6], [8]–[10], [16], [21], [32], [38]–[40].

Specifically, we conduct the experiments on three tracks, *i.e.*, (1) supervised learning (SL) track, (2) domain generalization (DG) track, and (3) cross-domain transfer learning (TL) track. The detailed settings of each track will be presented later. We use the common PSNR and SSIM [33] metrics to measure the performance of different methods. In addition, we present some visual results for subjective evaluation.

A. Supervised learning track

In this track, we compare different methods by training and testing them on our RealRain-1k-L and RealRain-1k-H, respectively. For each method, we use the original implementation code provided by the authors and adopt the same

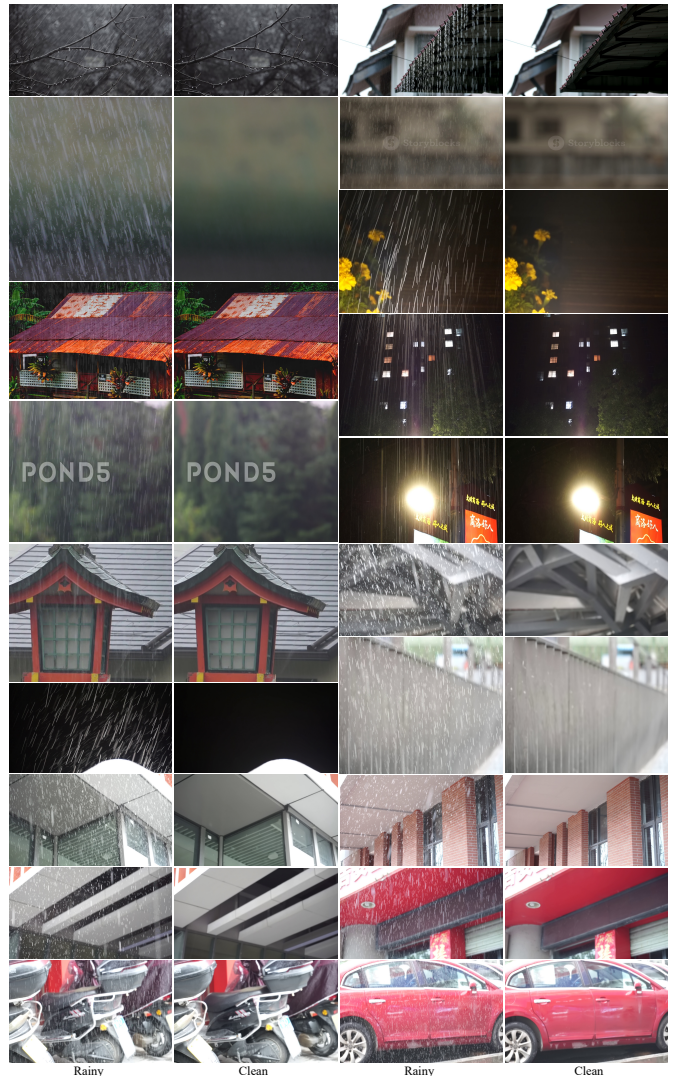


Fig. 6. More examples from our RealRain-1k.

training settings including augmentation, batch size, learning rate, optimizer, etc. We follow the common practice for all experiments, *i.e.*, all the methods are trained on the training set, validated on the validation set, and evaluated on the test set.

TABLE II
QUANTITATIVE RESULTS OF DIFFERENT SID METHODS ON REALRAIN-1K-L AND REALRAIN-1K-H.

Category	Method	RealRain-1k-H		RealRain-1k-L		Parameters (M)	FLOPs (G)
		PSNR (dB)	SSIM	PSNR (dB)	SSIM		
	Rainy images	22.27	0.7657	25.93	0.8651	-	-
Traditional	DSC [26]	24.48	0.7857	27.76	0.8750	-	-
	GMM [22]	24.93	0.8712	28.87	0.9259	-	-
CNNs	DDN [9]	29.17	0.8783	31.18	0.9172	0.06	7.41
	DerainNet [8]	22.88	0.8886	27.09	0.9250	0.75	88.29
	RESCAN [21]	29.39	0.8914	31.33	0.9261	0.15	32.32
	LPNet [10]	28.62	0.9424	32.47	0.9596	0.03	3.57
	SPANet [32]	25.76	0.9095	30.43	0.9470	0.28	36.25
	DRDNet [6]	30.78	0.9308	31.94	0.9426	5.23	689.84
	MSPFN [16]	25.08	0.8045	35.51	0.9668	21.00	708.44
	SPDNet [38]	26.63	0.8498	28.98	0.9005	3.32	96.61
	MPRNet [40]	34.74	0.9635	36.29	0.9721	3.64	141.45
	HINet [5]	40.82	0.9830	41.98	0.9869	88.67	170.71
Transformer	Restormer [39]	39.57	0.9812	40.90	0.9849	26.10	140.99

Main results The results as well as model size and FLOPs are summarized in Table II. As can be seen, the deep learning-based method of both architectures, *i.e.*, CNNs and transformers, significantly outperform the traditional prior-based methods on both RealRain-1k-H and RealRain-1k-L. The results validate the superiority of the deep neural networks, owing to their strong representation ability and the data-driven learning paradigm. When comparing CNN-based and the advanced transformer-based methods, Restormer outperforms MSPFN by a large margin, although they have the similar model size. Comparing the results of each method on RealRain-1k-H and RealRain-1k-L, we find that the performance of all the methods drops significantly when dealing with heavy rainy images. It shows that the proposed RealRain-1k-H and RealRain-1k-L have different levels of difficulties as implied by their names. It is noteworthy that our datasets can be easily extended to cover different levels of rain densities and it is interesting to investigate how different methods perform on rainy images with different rain densities, which we leave as our future work. Among all the methods, HINet achieves the best performance of 40.82 dB and 41.98 dB on RealRain-1k-H and RealRain-1k-L, respectively. However, it is also the largest model that has 88M parameters and high computational cost, *i.e.*, about 170G FLOPs. Therefore, it also matters to develop efficient SID methods that can achieve a better Pareto front between the deraining performance and model complexity.

Convergence comparison We select five representative methods to investigate their convergence performance by training them on RealRain-1k-L and RealRain-1k-H with different epochs, including 200, 500, 1000, and 2,000 epochs, respectively. For methods like Restormer that splits the training pipeline into several stages, we determine the training epochs in each stage proportionally.

The results are shown in Table III. As can be seen, except the smallest model, *i.e.*, DDN whose performance fluctuates in different settings, all other methods benefit from a longer

training schedule. When the model size increases, the model tends to have faster convergence speed owing to the stronger representation ability. For example, HINet trained with 200 and 500 epochs obtains comparable performance to MPRNet trained with 500 and 1000 epochs, respectively. An interesting finding is that the superiority of HINet over MPRNet diminishes with the increase of training epochs, where HINet is 20× larger than MPRNet. It implies that big models may have better data efficiency and it also matters to investigate the performance of different methods under the few-shot learning paradigm.

TABLE III
CONVERGENCE RESULTS ON REALRAIN-1K.

Training epochs	RealRain-1k-H				RealRain-1k-L				Parameters (M)
	200	500	1000	2000	200	500	1000	2000	
DDN [9]	29.00	29.42	27.37	28.64	31.22	32.13	30.23	32.88	0.06
RESCAN [21]	27.99	29.98	30.93	31.21	31.42	31.96	33.33	33.90	0.15
MPRNet [40]	32.80	35.90	37.63	39.68	34.60	37.84	39.64	41.34	3.64
HINet [5]	35.55	37.53	39.05	40.20	37.52	39.45	40.70	41.55	88.67
Restormer [39]	35.33	37.63	38.94	40.39	36.88	39.12	40.34	41.40	26.10

B. Domain generalization track

In this track, we quantitatively show the generalization performance of different methods, which are trained on a synthetic or real dataset and tested on an unseen real dataset. It is a common scenario when applying the developed SID methods in real-world applications, but has not been well studied. The experiments are conducted at two settings, *i.e.*, synthetic-to-real DG and real-to-real DG.

Synthetic-to-real DG We benchmark 11 deep learning-based methods based on the synthetic datasets, *i.e.*, Rain13k [16] and our SynRain-13k, and real datasets, *i.e.*, SPA-data [32], RainDS [27], and our RealRain-1k-L and RealRain-1k-H. All the methods are trained on the training set of these synthetic datasets and evaluated on the test sets

TABLE IV
QUANTITATIVE RESULTS OF REPRESENTATIVE SID METHODS ON THE SYNTHETIC-TO-REAL DG TRACK.

	Rain13k \rightarrow SPA-data		SynRain-13k \rightarrow SPA-data		Rain13k \rightarrow RainDS		SynRain-13k \rightarrow RainDS	
	PSNR (dB)	SSIM	PSNR (dB)	SSIM	PSNR (dB)	SSIM	PSNR (dB)	SSIM
Rainy images	32.63	0.9282	32.63	0.9282	21.80	0.6084	21.80	0.6084
DDN [9]	30.13	0.9132	31.22	0.9288	22.31	0.5973	22.92	0.6319
DerainNet [8]	30.78	0.9118	30.83	0.9259	21.35	0.5914	22.45	0.6446
RESCAN [21]	32.04	0.9385	33.50	0.9510	23.18	0.6499	23.82	0.6629
LPNet [10]	29.66	0.9201	31.10	0.9372	23.10	0.6429	23.29	0.6528
SPANet [32]	32.82	0.9337	33.81	0.9470	22.83	0.6289	23.21	0.6547
DRDNet [6]	28.35	0.8943	31.56	0.9403	22.78	0.6164	23.40	0.6513
MSPFN [16]	22.46	0.8952	34.89	0.9548	17.33	0.5865	23.60	0.6628
SPDNet [38]	32.44	0.9343	33.88	0.9531	23.41	0.6642	23.95	0.6706
MPRNet [40]	32.77	0.9396	35.08	0.9555	23.25	0.6563	23.82	0.6686
HINet [5]	32.35	0.9361	34.62	0.9521	23.50	0.6639	23.91	0.6683
Restormer [39]	32.65	0.9358	35.48	0.9586	22.96	0.6480	24.03	0.6711

TABLE V
QUANTITATIVE RESULTS OF REPRESENTATIVE SID METHODS ON THE SYNTHETIC-TO-REAL DG TRACK.

	Rain13k \rightarrow RealRain-1k-H		SynRain-13k \rightarrow RealRain-1k-H		Rain13k \rightarrow RealRain-1k-L		SynRain-13k \rightarrow RealRain-1k-L	
	PSNR (dB)	SSIM	PSNR (dB)	SSIM	PSNR (dB)	SSIM	PSNR (dB)	SSIM
Rainy images	22.27	0.7657	22.27	0.7657	25.93	0.8651	25.93	0.8651
DDN [9]	27.00	0.8468	26.06	0.8270	29.94	0.9047	29.89	0.9016
DerainNet [8]	21.91	0.7420	23.50	0.8483	25.40	0.8474	27.29	0.9138
RESCAN [21]	25.32	0.8591	28.66	0.9057	28.98	0.9178	32.55	0.9460
LPNet [10]	26.66	0.8824	27.54	0.8934	28.97	0.9207	31.16	0.9373
SPANet [32]	24.17	0.8304	24.96	0.8440	27.40	0.8959	30.33	0.9399
DRDNet [6]	25.05	0.8131	27.42	0.8801	27.03	0.8634	31.27	0.9316
MSPFN [16]	17.92	0.7728	30.05	0.9399	19.50	0.8552	34.44	0.9678
SPDNet [38]	24.63	0.8585	29.78	0.9272	27.94	0.9111	33.69	0.9590
MPRNet [40]	23.39	0.8346	30.32	0.9402	26.51	0.8949	34.40	0.9646
HINet [5]	23.82	0.8382	30.66	0.9390	26.56	0.8920	34.74	0.9651
Restormer [39]	23.13	0.8152	31.89	0.9485	26.29	0.8825	35.90	0.9703

of these real datasets, following the original settings in their papers. We use the models trained on Rain13k from their official repositories if provided.

The results are summarized in Table IV, Figure 7 show some visual examples. As can be seen, when trained on SynRain-13k and tested on both SPA-data and RainDS, all the methods have better generalization performance than those trained on Rain13k. The results demonstrate the value of the proposed SynRain-13k which is generated using the real rain layers and has a smaller synthetic to real domain gap. Besides, Restormer trained on SynRain-13k achieves the best generalization performance in all scenarios, validating the good generalization ability of transformer as studied in [41].

We also show the generalization performance of different methods on the test sets of our RealRain-1k-H and RealRain-1k-L. As shown in Table V, the models trained on our SynRain-13k generalize better on RealRain-1k, which is consistent with the results in Table IV, validating the value of the proposed SynRain-13k.

Real-to-real DG We benchmark three most representative SID methods in this track based on RealRain-1k-H, RealRain-1k-L, and SPA-data, whose rain density decreases in order. The models trained on RealRain-1k are collected from the experiments in Table II, while the models trained on SPA-data are collected from the official repositories or retrained

following the same setting.

The results are summarized in Table VI. Comparing Table VI and Table IV, we can see that our RealRain-1k datasets can help methods generalize well to an unseen real domain. For example, both Restormer and HINet in the RealRain-1k-L \rightarrow SPA-data setting perform better than the counterparts in the Rain13k \rightarrow SPA-data setting. It is also interesting to find that the methods trained on our SynRain-13k outperform those trained on our RealRain-1k, owing to the real rain layers and large data volume of SynRain-13k. Besides, the experiment results also show that the generalization performance decreases when the difference of rain density in training and test sets becomes larger. For example, the methods in RealRain-1k-L \rightarrow SPA-data generalize better than those in RealRain-1k-H \rightarrow SPA-data. We also show some visual examples in Figure 8. The promising deraining results further validate the value and effectiveness of RealRain-1k.

To better reveal how and why the models behave differently when encountering the different rain density gap. We conduct several experiments to further support our claim. We split each test image into two non-overlapped regions according to the difference threshold between the rainy image and groundtruth, *i.e.*, rainy region and rain-free region, where the rainy region denotes the area whose difference is above the threshold. We show the restoration performance on the two kinds of regions

TABLE VI
 QUANTITATIVE RESULTS OF REPRESENTATIVE SID METHODS ON THE REAL-TO-REAL DG TRACK.

	RealRain-1k-L \rightarrow SPA-data		RealRain-1k-H \rightarrow SPA-data		SPA-data \rightarrow RealRain-1k-L		SPA-data \rightarrow RealRain-1k-H	
	PSNR (dB)	SSIM						
Rainy images	32.63	0.9282	32.63	0.9282	25.93	0.8651	22.27	0.7657
MPRNet [40]	32.50	0.9482	30.70	0.9360	31.14	0.9519	27.96	0.9199
HINet [5]	35.37	0.9634	34.08	0.9575	32.45	0.9586	28.62	0.9225
Restormer [39]	33.84	0.9590	32.93	0.9545	33.45	0.9687	28.69	0.9337



Fig. 7. Visual comparison of three representative methods MSPFN [16], MPRNet [40] and Restormer [39] trained on the Rain13k and our SynRain-13k respectively.

TABLE VII
THE PERFORMANCE GAIN OF RAINY REGION AND RAIN-FREE REGION WHEN REALRAIN-1K-H/L GENERALIZE TO SPA-DATA.

RealRain-1k-H \rightarrow SPA-data	Rainy region PSNR (dB)	Rain-free region PSNR (dB)	RealRain-1k-L \rightarrow SPA-data	Rainy region PSNR (dB)	Rain-free region PSNR (dB)
Rainy images	22.96	37.34	Rainy images	22.96	37.34
MPRNet [40]	26.95	30.65	MPRNet [40]	26.83	33.31
Gain	3.99	-6.68	Gain	3.87	-4.02
Restormer [39]	27.59	31.60	Restormer [39]	27.83	32.71
Gain	4.63	-5.74	Gain	4.87	-4.62

TABLE VIII
THE PERFORMANCE GAIN OF RAINY REGION AND RAIN-FREE REGION WHEN SPA-DATA GENERALIZE TO REALRAIN-1K-H/L.

SPA-data \rightarrow RealRain-1k-H	Rainy region PSNR (dB)	Rain-free region PSNR (dB)	SPA-data \rightarrow RealRain-1k-L	Rainy region PSNR (dB)	Rain-free region PSNR (dB)
Rainy images	22.72	29.38	Rainy images	23.72	31.15
MPRNet [40]	25.73	31.78	MPRNet [40]	27.39	33.47
Gain	3.01	2.40	Gain	3.67	2.32
Restormer [39]	25.21	31.23	Restormer [39]	27.88	33.33
Gain	2.49	1.85	Gain	4.16	2.18

in the following Table VII and Table VIII. It can be seen that the generalization performance from heavy rain to light rain is better in the rainy regions but affected by the unsatisfactory generalization ability in the rain-free regions. Specifically, when comparing RealRain-1k-H \rightarrow SPA-data and RealRain-1k-L \rightarrow SPA-data, the performance gain in rainy regions remains similar while there is a significant difference in the rain-free regions. This is because that the rain streaks cover more regions for those images with higher rain density. When handling the light rainy images where rain-free regions dominate, the model trained with RealRain-1k-H may remove rain-like structures in the rain-free regions, *e.g.*, an unpleasant result of model overfitting. Therefore, it affects the overall gain brought by rain removal, leading to a relatively small PSNR improvement. In other word, it is caused by the limited generalization ability of deraining models due to domain gap between the training set and test set. The results in Table VI also demonstrate this claim, where the performance gain of RealRain-1k-L \rightarrow SPA-data is larger than RealRain-1k-H \rightarrow SPA-data, and the models trained on SPA-data perform better on RealRain-1k-L than RealRain-1k-H, especially for Restormer. On the contrary, the model trained using light rainy images like SPA-data learns to recover only a small part of the images and tends to reserve most regions by regarding them as rain-free ones when dealing with the heavy rainy images. Consequently, the generalizing performance of all models from SPA-data to RealRain-1k-H reaches no more than 28.7dB, which is unsatisfactory because only part of rain streaks are removed.

Our DG experiments reveal that the models behave differently when generalizing from heavy to light and light to heavy, *i.e.*, models trained on light rain images can obtain larger performance gain when generalizing to heavy rain images, while the model generalizing from heavy to light tends to change the details of the rain-free region, resulting in relatively lower improvement. These findings have never been revealed by previous works, owing to the comparisons on

the proposed rain density-controllable dataset. It confirms the value of our proposed dataset. Besides, it is also noteworthy that the proposed RealRain-1k-L and RealRain-1k-H are more challenging than the SPA-data since their rainy images have smaller PSNR values due to the larger rain density. As shown in Table VI in the paper, the performance is far from saturation on the RealRain-1k-H dataset, calling for more research efforts on image deraining, especially for heavy rain images.

Real-to-real DG with different training schedules The results on the setting of real-to-real domain generalization with different training schedules are shown in Table IX and Table X. As can be seen, the generalization performance on the SPA-data is getting better with the increase of training epochs on our RealRain-1k dataset. Again, the results confirm the value of our dataset for training a better model that generalizes well to real rainy images. It is noteworthy that the results of different methods in Table IX and Table X are not consistent with those in Table VI, because we train them according to their default settings (*i.e.*, with different training epochs for different methods) for the experiment in Table VI.

C. Cross-domain transfer learning track

In this track, we compare two representative methods, *i.e.*, MPRNet [40] and Restormer [39] on different settings. Compared to the synthetic-to-real DG setting, we collect the models trained on the synthetic datasets including Rain13k and SynRain-13k, and further fine-tune them on the training sets of SPA-data, RainDS, RealRain-1k-H, and RealRain-1k-L. The results are given in Table XI. Again, both methods pre-trained on our SynRain-13k outperform those pre-trained on Rain13k or without pre-training, showing the benefit of the real rain layers. And the results after fine-tuning are much better than those in the synthetic-to-real and real-to-real DG settings, which is reasonable since the training data from the downstream datasets are used. Note that the performances of Restormer [39] pre-trained on the synthetic datasets are

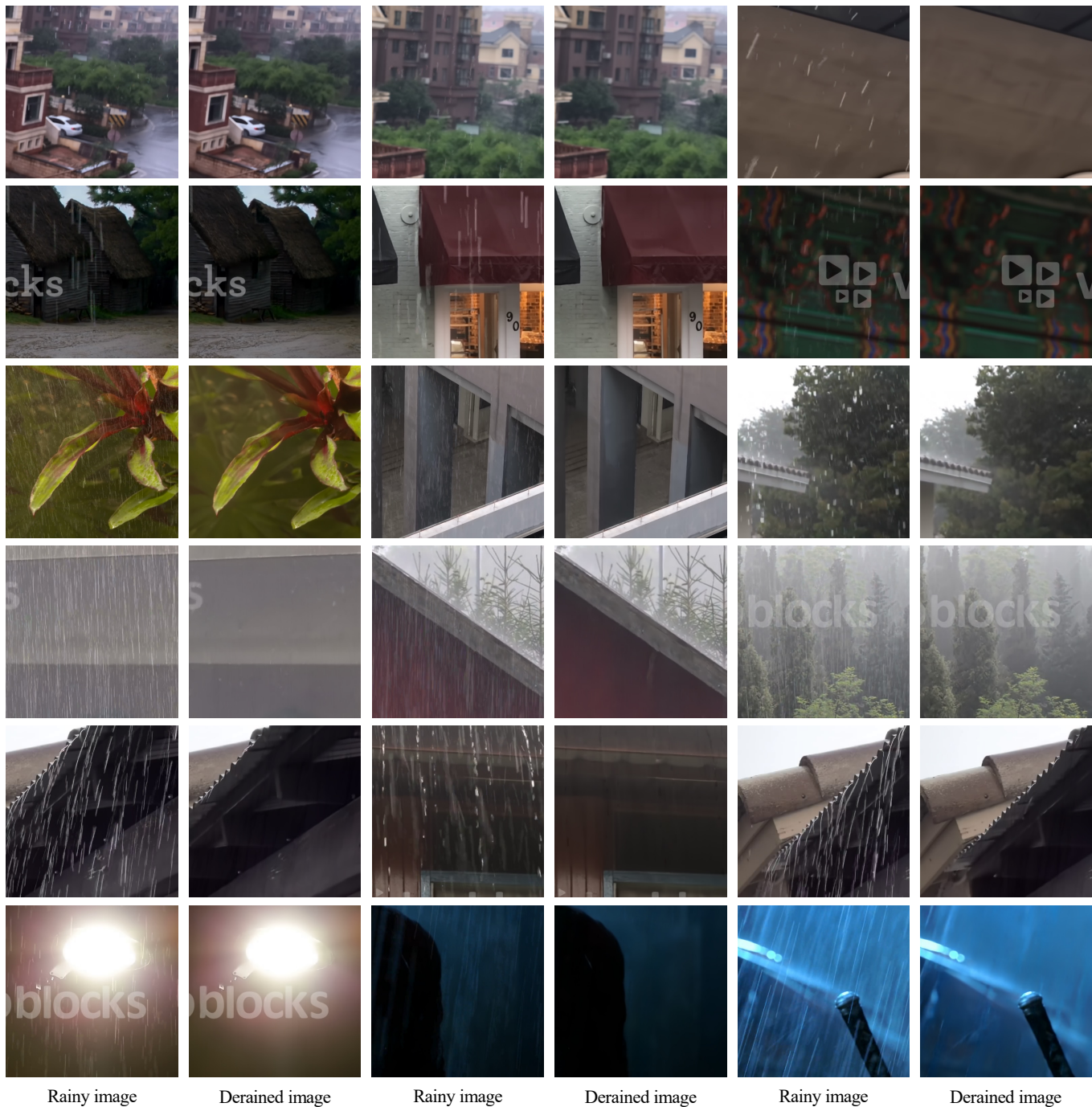


Fig. 8. Some deraining results of HINet [5] which is trained on our RealRain-1k-L and evaluated on SPA-data [32]. We can see that the deraining results are fairly promising demonstrating that our datasets can generalize to various rainy scenarios.

TABLE IX
REALRAIN-1K-L \rightarrow SPA-DATA DOMAIN GENERALIZATION WITH DIFFERENT TRAINING SCHEDULES.

Training epochs	RealRain-1k-L \rightarrow SPA-data							
	200		500		1000		2000	
	PSNR (dB)	SSIM	PSNR (dB)	SSIM	PSNR (dB)	SSIM	PSNR (dB)	SSIM
Rainy images	32.63	0.9282	32.63	0.9282	32.63	0.9282	32.63	0.9282
MPRNet [40]	30.94	0.9391	33.10	0.9512	33.63	0.9529	34.73	0.9601
HINet [5]	32.91	0.9489	34.26	0.9556	34.74	0.9593	35.14	0.9623
Restormer [39]	32.75	0.9451	33.49	0.9545	33.65	0.9575	34.52	0.9623

TABLE X
REALRAIN-1K-H→SPA-DATA DOMAIN GENERALIZATION WITH DIFFERENT TRAINING SCHEDULES.

Training epochs	RealRain-1k-H → SPA-data							
	200		500		1000		2000	
	PSNR (dB)	SSIM	PSNR (dB)	SSIM	PSNR (dB)	SSIM	PSNR (dB)	SSIM
Rainy images	32.63	0.9282	32.63	0.9282	32.63	0.9282	32.63	0.9282
MPRNet [40]	28.56	0.9175	31.80	0.9446	32.11	0.9455	34.01	0.9568
HINet [5]	30.44	0.9326	32.13	0.9455	33.37	0.9516	33.75	0.9555
Restormer [39]	31.65	0.937	33.19	0.9508	33.14	0.9525	33.92	0.9590

TABLE XI
RESULTS ON THE CROSS-DOMAIN TRANSFER LEARNING TRACK.

Method	Test set	Pre-training dataset					
		N/A		Rain13k		SynRain-13k	
		PSNR (dB)	SSIM	PSNR (dB)	SSIM	PSNR (dB)	SSIM
MPRNet [40]	SPA-data	39.73	0.9799	44.40	0.9881	44.91	0.9888
	RainDS	23.59	0.6498	25.48	0.7101	25.65	0.7107
	RealRain-1k-H	34.74	0.9635	38.48	0.9795	38.98	0.9807
	RealRain-1k-L	33.47	0.9592	40.64	0.9844	41.35	0.9867
Restormer [39]	SPA-data	46.87	0.9903	46.02	0.9904	46.14	0.9905
	RainDS	25.10	0.6982	25.62	0.7153	25.79	0.7165
	RealRain-1k-H	39.57	0.9812	41.63	0.9869	41.88	0.9872
	RealRain-1k-L	40.90	0.9849	42.76	0.9890	43.01	0.9895

inferior to the one without pre-training. Maybe it is because the backgrounds in the training set of SPA-data overlap with the ones in the test set. Therefore, Restormer could achieve a very good performance even without pre-training.

D. Model complexity

The model complexity of different methods is shown in Table XII, including model parameters, FLOPs, GPU memory footprint, and inference latency. From the table, we can see that the model size, the latency and FLOPs increase in recent years, probably due to the advance of GPUs and the trend of pursuing better performance. For example, MPRNet needs about 3s to process an image, while HINet has 88M parameters, limiting their usage in practical applications. Therefore, it deserves more research efforts to achieve a better balance between deraining performance and model complexity.

TABLE XII

MODEL COMPLEXITY OF REPRESENTATIVE SID METHODS. THE FLOPS ARE CALCULATED GIVEN A TEST IMAGE OF 256×256 RESOLUTION. THE GPU MEMORY AND LATENCY ARE CALCULATED WHEN PROCESSING AN IMAGE OF 512×512 RESOLUTION. ALL RESULTS ARE OBTAINED ON THE SAME GTX 1080 T1 GPU.

Method	Venue	Params. (M)	FLOPs (G)	Memory (G)	Latency (ms)
DDN [9]	CVPR'17	0.058	7.407	3.40	24.28
DerainNet [8]	TIP'17	0.750	88.287	4.40	64.00
RESCAN [21]	ECCV'18	0.150	32.320	1.10	103.83
LPNet [10]	TNNLS'19	0.027	3.566	8.10	471.00
SPANet [32]	CVPR'19	0.284	36.250	1.08	1103.20
DRDNet [6]	CVPR'20	5.230	689.840	10.70	888.39
MSPFN [16]	CVPR'20	21.000	708.437	10.70	656.20
SPDNet [38]	ICCV'21	3.320	96.610	1.89	269.66
MPRNet [40]	CVPR'21	3.640	141.450	1.67	2901.00
HINet [5]	CVPRW'21	88.666	170.714	1.97	826.86
Restormer [39]	CVPR'22	26.097	140.990	3.98	1684.93

V. CONCLUSION AND DISCUSSION

In this paper, we establish a high-quality real rainy dataset RealRain-1k using a simple but effective rain density-controllable filtering method and a large-scale synthetic dataset SynRain-13k based on real rain layers. Based on them, we benchmark more than 10 deraining methods comprehensively on three tracks. The results demonstrate the value of the proposed datasets, the different representation abilities of CNNs- or transformers-based methods, and the generalization performance under different learning paradigms with different datasets. We hope RealRain-1k and SynRain-13k can serve as test beds to facilitate future research in this area.

Limitation and discussion Our real dataset only has 1k images in the current version, which can be scaled up by collecting more videos. Meanwhile, more rainy images of different rain densities can be generated to form a series of datasets, each of which has a specific level of rain density.

Social impact. RealRain-1k and SynRain-13k can benefit the study of image deraining that is of great practical significance. Attention should be drawn to the generalization ability of models trained on our datasets, which may not be good in unseen scenes with extremely different rain streaks.

REFERENCES

- [1] N. Ahn, S. Y. Jo, and S.-J. Kang. Eagnet: Elementwise attentive gating network-based single image de-raining with rain simplification. *IEEE Transactions on Circuits and Systems for Video Technology*, 32(2):608–620, 2021.
- [2] L. Cai, Y. Fu, W. Huo, Y. Xiang, T. Zhu, Y. Zhang, H. Zeng, and D. Zeng. Multi-scale attentive image de-raining networks via neural architecture search. *IEEE Transactions on Circuits and Systems for Video Technology*, 2022.

- [3] Q. Cai, Y. Qian, J. Li, J. Lv, Y.-H. Yang, F. Wu, and D. Zhang. Hippa: Hierarchical patch transformer for single image super resolution. *arXiv preprint arXiv:2203.10247*, 2022.
- [4] H. Chen, Y. Wang, T. Guo, C. Xu, Y. Deng, Z. Liu, S. Ma, C. Xu, C. Xu, and W. Gao. Pre-trained image processing transformer. In *Proceedings of the IEEE/CVF Conference on Computer Vision and Pattern Recognition*, pages 12299–12310, 2021.
- [5] L. Chen, X. Lu, J. Zhang, X. Chu, and C. Chen. Hinet: Half instance normalization network for image restoration. In *Proceedings of the IEEE/CVF Conference on Computer Vision and Pattern Recognition*, pages 182–192, 2021.
- [6] S. Deng, M. Wei, J. Wang, Y. Feng, L. Liang, H. Xie, F. L. Wang, and M. Wang. Detail-recovery image deraining via context aggregation networks. In *Proceedings of the IEEE/CVF conference on computer vision and pattern recognition*, pages 14560–14569, 2020.
- [7] A. Dosovitskiy, L. Beyer, A. Kolesnikov, D. Weissenborn, X. Zhai, T. Unterthiner, M. Dehghani, M. Minderer, G. Heigold, S. Gelly, et al. An image is worth 16x16 words: Transformers for image recognition at scale. In *International Conference on Learning Representations*, 2020.
- [8] X. Fu, J. Huang, X. Ding, Y. Liao, and J. Paisley. Clearing the skies: A deep network architecture for single-image rain removal. *IEEE Transactions on Image Processing*, 26(6):2944–2956, 2017.
- [9] X. Fu, J. Huang, D. Zeng, Y. Huang, X. Ding, and J. Paisley. Removing rain from single images via a deep detail network. In *Proceedings of the IEEE conference on computer vision and pattern recognition*, pages 3855–3863, 2017.
- [10] X. Fu, B. Liang, Y. Huang, X. Ding, and J. Paisley. Lightweight pyramid networks for image deraining. *IEEE transactions on neural networks and learning systems*, 31(6):1794–1807, 2019.
- [11] K. Garg and S. K. Nayar. Photorealistic rendering of rain streaks. *ACM Transactions on Graphics (TOG)*, 25(3):996–1002, 2006.
- [12] K. Garg and S. K. Nayar. Vision and rain. *International Journal of Computer Vision*, 75(1):3–27, 2007.
- [13] X. Hu, C.-W. Fu, L. Zhu, and P.-A. Heng. Depth-attentional features for single-image rain removal. In *Proceedings of the IEEE/CVF Conference on Computer Vision and Pattern Recognition*, pages 8022–8031, 2019.
- [14] H. Ji, X. Feng, W. Pei, J. Li, and G. Lu. U2-former: A nested u-shaped transformer for image restoration. *arXiv preprint arXiv:2112.02279*, 2021.
- [15] K. Jiang, Z. Wang, P. Yi, C. Chen, Z. Han, T. Lu, B. Huang, and J. Jiang. Decomposition makes better rain removal: An improved attention-guided deraining network. *IEEE Transactions on Circuits and Systems for Video Technology*, 31(10):3981–3995, 2020.
- [16] K. Jiang, Z. Wang, P. Yi, C. Chen, B. Huang, Y. Luo, J. Ma, and J. Jiang. Multi-scale progressive fusion network for single image deraining. In *Proceedings of the IEEE/CVF conference on computer vision and pattern recognition*, pages 8346–8355, 2020.
- [17] L.-W. Kang, C.-W. Lin, and Y.-H. Fu. Automatic single-image-based rain streaks removal via image decomposition. *IEEE transactions on image processing*, 21(4):1742–1755, 2011.
- [18] M. Kumar, D. Weissenborn, and N. Kalchbrenner. Colorization transformer. In *International Conference on Learning Representations*, 2020.
- [19] Y. LeCun, Y. Bengio, and G. Hinton. Deep learning. *nature*, 521(7553):436–444, 2015.
- [20] R. Li, L.-F. Cheong, and R. T. Tan. Heavy rain image restoration: Integrating physics model and conditional adversarial learning. In *Proceedings of the IEEE/CVF Conference on Computer Vision and Pattern Recognition*, pages 1633–1642, 2019.
- [21] X. Li, J. Wu, Z. Lin, H. Liu, and H. Zha. Recurrent squeeze-and-excitation context aggregation net for single image deraining. In *Proceedings of the European conference on computer vision (ECCV)*, pages 254–269, 2018.
- [22] Y. Li, R. T. Tan, X. Guo, J. Lu, and M. S. Brown. Rain streak removal using layer priors. In *Proceedings of the IEEE conference on computer vision and pattern recognition*, pages 2736–2744, 2016.
- [23] J. Liang, J. Cao, G. Sun, K. Zhang, L. Van Gool, and R. Timofte. Swinir: Image restoration using swin transformer. In *Proceedings of the IEEE/CVF International Conference on Computer Vision*, pages 1833–1844, 2021.
- [24] L. Liu, L. Xie, X. Zhang, S. Yuan, X. Chen, W. Zhou, H. Li, and Q. Tian. Tape: Task-agnostic prior embedding for image restoration. *arXiv preprint arXiv:2203.06074*, 2022.
- [25] Y. Liu, Z. Yue, J. Pan, and Z. Su. Unpaired learning for deep image deraining with rain direction regularizer. In *Proceedings of the IEEE/CVF International Conference on Computer Vision*, pages 4753–4761, 2021.
- [26] Y. Luo, Y. Xu, and H. Ji. Removing rain from a single image via discriminative sparse coding. In *Proceedings of the IEEE international conference on computer vision*, pages 3397–3405, 2015.
- [27] R. Quan, X. Yu, Y. Liang, and Y. Yang. Removing raindrops and rain streaks in one go. In *Proceedings of the IEEE/CVF Conference on Computer Vision and Pattern Recognition*, pages 9147–9156, 2021.
- [28] D. Ren, W. Zuo, Q. Hu, P. Zhu, and D. Meng. Progressive image deraining networks: A better and simpler baseline. In *Proceedings of the IEEE/CVF Conference on Computer Vision and Pattern Recognition*, pages 3937–3946, 2019.
- [29] A. Vaswani, N. Shazeer, N. Parmar, J. Uszkoreit, L. Jones, A. N. Gomez, L. Kaiser, and I. Polosukhin. Attention is all you need. *Advances in neural information processing systems*, 30, 2017.
- [30] G. Wang, C. Sun, and A. Sowmya. Context-enhanced representation learning for single image deraining. *International Journal of Computer Vision*, 129(5):1650–1674, 2021.
- [31] H. Wang, Q. Xie, Q. Zhao, and D. Meng. A model-driven deep neural network for single image rain removal. In *Proceedings of the IEEE/CVF Conference on Computer Vision and Pattern Recognition*, pages 3103–3112, 2020.
- [32] T. Wang, X. Yang, K. Xu, S. Chen, Q. Zhang, and R. W. Lau. Spatial attentive single-image deraining with a high quality real rain dataset. In *Proceedings of the IEEE/CVF Conference on Computer Vision and Pattern Recognition*, pages 12270–12279, 2019.
- [33] Z. Wang, A. C. Bovik, H. R. Sheikh, and E. P. Simoncelli. Image quality assessment: from error visibility to structural similarity. *IEEE transactions on image processing*, 13(4):600–612, 2004.
- [34] Z. Wang, X. Cun, J. Bao, and J. Liu. Uformer: A general u-shaped transformer for image restoration. *arXiv preprint arXiv:2106.03106*, 2021.
- [35] F. Yang, H. Yang, J. Fu, H. Lu, and B. Guo. Learning texture transformer network for image super-resolution. In *Proceedings of the IEEE/CVF conference on computer vision and pattern recognition*, pages 5791–5800, 2020.
- [36] W. Yang, R. T. Tan, J. Feng, J. Liu, Z. Guo, and S. Yan. Deep joint rain detection and removal from a single image. In *Proceedings of the IEEE conference on computer vision and pattern recognition*, pages 1357–1366, 2017.
- [37] R. Yasarla and V. M. Patel. Uncertainty guided multi-scale residual learning-using a cycle spinning cnn for single image de-raining. In *Proceedings of the IEEE/CVF Conference on Computer Vision and Pattern Recognition*, pages 8405–8414, 2019.
- [38] Q. Yi, J. Li, Q. Dai, F. Fang, G. Zhang, and T. Zeng. Structure-preserving deraining with residue channel prior guidance. In *Proceedings of the IEEE/CVF International Conference on Computer Vision*, pages 4238–4247, 2021.
- [39] S. W. Zamir, A. Arora, S. Khan, M. Hayat, F. S. Khan, and M.-H. Yang. Restormer: Efficient transformer for high-resolution image restoration. *arXiv preprint arXiv:2111.09881*, 2021.
- [40] S. W. Zamir, A. Arora, S. Khan, M. Hayat, F. S. Khan, M.-H. Yang, and L. Shao. Multi-stage progressive image restoration. In *Proceedings of the IEEE/CVF Conference on Computer Vision and Pattern Recognition*, pages 14821–14831, 2021.
- [41] C. Zhang, M. Zhang, S. Zhang, D. Jin, Q. Zhou, Z. Cai, H. Zhao, S. Yi, X. Liu, and Z. Liu. Delving deep into the generalization of vision transformers under distribution shifts. *arXiv preprint arXiv:2106.07617*, 2021.
- [42] H. Zhang and V. M. Patel. Convolutional sparse and low-rank coding-based rain streak removal. In *2017 IEEE Winter conference on applications of computer vision (WACV)*, pages 1259–1267. IEEE, 2017.
- [43] H. Zhang and V. M. Patel. Density-aware single image de-raining using a multi-stream dense network. In *Proceedings of the IEEE conference on computer vision and pattern recognition*, pages 695–704, 2018.
- [44] H. Zhang, V. Sindagi, and V. M. Patel. Image de-raining using a conditional generative adversarial network. *IEEE transactions on circuits and systems for video technology*, 30(11):3943–3956, 2019.
- [45] J. Zhang and D. Tao. Empowering things with intelligence: a survey of the progress, challenges, and opportunities in artificial intelligence of things. *IEEE Internet of Things Journal*, 8(10):7789–7817, 2020.
- [46] L. Zhu, Z. Deng, X. Hu, H. Xie, X. Xu, J. Qin, and P.-A. Heng. Learning gated non-local residual for single-image rain streak removal. *IEEE Transactions on Circuits and Systems for Video Technology*, 31(6):2147–2159, 2020.
- [47] L. Zhu, C.-W. Fu, D. Lischinski, and P.-A. Heng. Joint bi-layer optimization for single-image rain streak removal. In *Proceedings of the IEEE international conference on computer vision*, pages 2526–2534, 2017.